III International Conference on Particle-based Methods – Fundamentals and Applications
PARTICLES 2013
M. Bischoff, E. Oñate, D.R.J. Owen, E. Ramm & P. Wriggers (Eds)

MODELLING OF BEHAVIOUR OF PLAIN CONCRETE USING DEM

M. NITKA[1] AND J. TEJCHMAN[2]

[1]Gdańsk University of Technology
80-233 Gdańsk-Wrzeszcz, Narutowicza 11/12
micnitka@pg.gda.pl

[2]Gdańsk University of Technology
80-233 Gdańsk-Wrzeszcz, Narutowicza 11/12
tejchmk@pg.gda.pl

Key words: Aggregate, Cement, Concrete, DEM, Micro-structure.

Abstract. For a realistic description of the mechanical behaviour of concrete, which is a strongly inhomogeneous and non-linear, microstructure should be taken into account. The size, volume and shape of aggregate have a pronounced influence on the concrete behaviour at the macro-level. In this paper, the discrete element method (DEM) is used as a tool to describe the concrete behaviour under uniaxial compression and uniaxial tension.

1 INTRODUCTION

To model realistically the behaviour of concrete, its micro-structure should be taken into account. It can be achieved by means of the discrete element method DEM [1-5]. The method is based on modelling of aggregate particles and cement matrix particles as rigid discrete elements, which interact with each according to a tangential contact elasto-plastic Mohr-Coulomb law with cohesion and an elastic normal contact law.

The existing DEM models for concrete indicate some disadvantages as e.g.: they use a non-physical aggregate distribution and aggregate size or they use an additional degradation term to obtain a more smooth response of concrete in a post-peak regime. Our goal is to describe the concrete behaviour at the global level in agreement with laboratory tests by taking its realistic internal structure into account.

In this paper we studied the concrete behaviour under uniaxial compression and uniaxial tension with spherical elements. The influence of the aggregate size and aggregate volume, the specimen thickness and the presence of interfacial transitional zones was investigated on the global behaviour. The discrete modelling results were directly compared with the corresponding experimental tests results.

2 DISCRETE ELEMENT METHODS FOR CONCRETE

To simulate the behaviour of concrete, a three-dimensional spherical discrete model YADE, developed at University of Grenoble [6,7], was used by taking into account the so-called soft-particle approach (i.e. the model allows for particle deformation - modelled as an

overlap of particles). The aggregate and cement matrix structure was modelled as spheres. The force vector $\vec{F}$ between spheres in contact was decomposed into two vectors: a normal and tangential one. The normal and tangential forces were linked to the displacements through the normal stiffness K_n and tangential stiffness K_s (Figs.1a and 1b)

$$\vec{F}_n = K_n U \vec{N}, \tag{1}$$

$$\vec{F}_s = \vec{F}_s + K_s \Delta \vec{X}_s + F_s^{max}, \tag{2}$$

where U is the overlap between spheres, $\vec{N}$ denotes the normal vector at the contact point, $\Delta \vec{X}_s$ is the incremental tangential displacement and F_s^{max} is the cohesive force between particles.

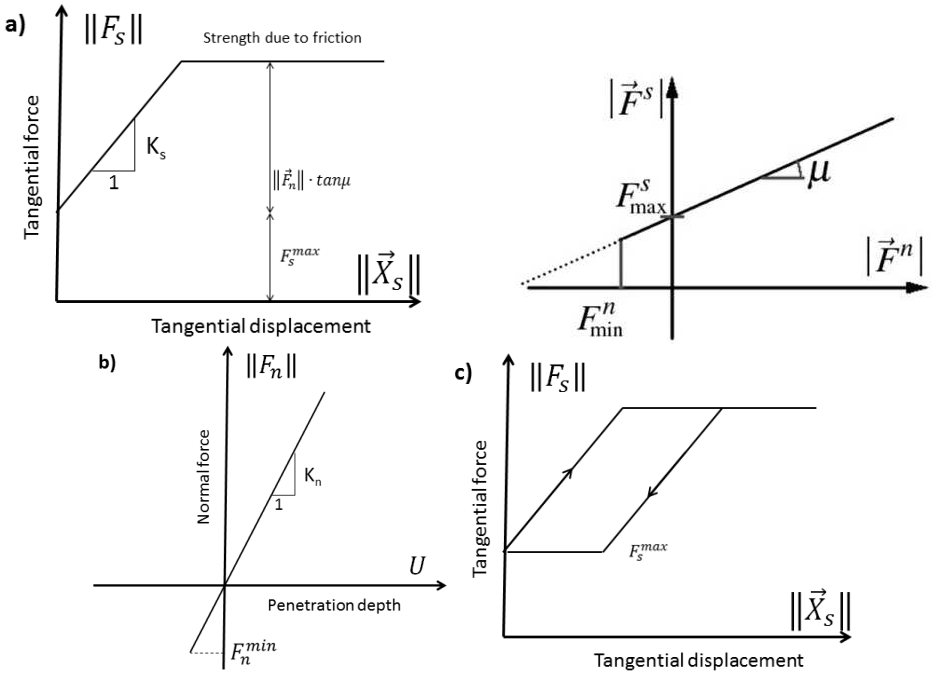

Figure 1: Mechanical response of DEM: a) tangential contact model, b) normal contact model and c) loading and unloading path in tangential contact model

The stiffness parameters were computed with the aid of the modulus of elasticity of the grain contact E_c and two neighbouring grain radii R_A and R_B (to determine the normal stiffness K_n) and with the aid of the modulus of elasticity E_c and Poisson's ratio ν_c of the grain contact and two neighbouring grain radii R_A and R_B (to determine the tangential stiffness K_s), respectively

$$K_n = E_c \frac{2R_A R_B}{R_A + R_B} \quad \text{and} \quad K_s = \nu_c E_c \frac{2R_A R_B}{R_A + R_B}. \tag{3}$$

If the grain radius $R_A = R_B = R$, the stiffness parameters were equal to: $K_n = E_c R$ and $K_s = \nu_c E_c R$, respectively (thus $K_s/K_n = \nu_c$). The frictional sliding started at the contact point if the contact forces $\vec{F}_s$ and $\vec{F}_n$ satisfied the frictional Mohr-Coulomb equation (Fig.1a)

$$\|\vec{F}_s\| \leq F_s^{max} + \|\vec{F}_n\| \times \tan\mu, \tag{4}$$

where μ denotes the inter-particle friction angle. The normal force may be negative even if a geometrical contact between elements does not exist. When spheres are separated, the normal force is negative up to the minimum value F_n^{min}($\|\vec{F}_n\| \geq F_n^{min}$); later the contact between spheres is completely broken and no forces are transmitted. If the contact between grains again happens, no cohesion between them is considered afresh. A choice of a very simple linear elastic normal contact (Fig.1b) was intended to capture in average various contact possibilities possible in real concrete. The following five main local material parameters were needed for discrete simulations: E_c, ν_c, μ, F_n^{min} and F_s^{max}. In addition, the particle radius R, particle density ρ and damping parameters α were required.

3 DISCRETE RESULTS OF CONCRETE SAMPLES

The discrete simulations were manly carried out under quasi-static 2D conditions with the specimen depth equal to the aggregate grain size (i.e. only one aggregate particle layer was simulated in the perpendicular plane) in order to significantly accelerate calculations. Aggregate and cement matrix were modelled as rigid spheres of a different diameter. The friction angle μ was assumed as μ=30^o, (ρ=2500 kg/m^3). The contact modulus of elasticity was mainly E_c=60 GPa and the contact Poisson's ratio ν_c=0.2. The cohesive force was equal $F_s^{max} = Cr_{min}^2$ and the tensile force $F_n^{min} = T\, r_{min}^2$, where C – the maximum shear stress , T – the minimum normal stress and r_{min} - the minimum radius of spheres in contact. For compression tests , the specimen 10×10 cm^2 was assumed (Fig.2a) and for tension tests the 'dog-bone' specimen (height 15cm, width 10cm on the top and bottom and 6 cm in the mid-height) was chosen (Fig.2b) to compare discrete results with corresponding laboratory experiments by van Vliet and van Mier [8,9]. Spheres were non-uniformly distributed with a random diameter, mainly between d_{min}=1.0 mm and d_{max}=12mm, and with the mean diameter of d_{50}=2 mm. The top and bottom of specimens was smooth without wall friction. First, particles were randomly distributed inside specimens. Second, after relaxation, all forces acting on particles were removed before deformation along the specimen top was prescribed.

3.1 Influence of initial porosity

Five different specimens were modelled. The specimen area of 75% was always covered by aggregate spheres with the diameter larger than 2 mm. Then, cement matrix spheres with the diameter below 2 mm were added as p=90%, 95%, 100% and 125%, respectively ($p = \frac{p_d}{p_s}$[%], where p_d - the area of aggregate particles and p_s - the specimen area). If $p \geq$100%, there already exist some overlaps between particles, which are not taken into account if deformation is prescribed. The number of spheres in a specimen under compression was 3992, 5016, 6048 and 11168 and in a specimen under tension 4935, 6206, 7266 and 13193. The minimum sphere diameter was d_{min}=1 mm with C=160 MPa and T=90 MPa.

Figure 3 shows the calculated evolution of the vertical normal stress σ_{yy} versus the vertical normal strain ε_{yy} as compared to experiments. The higher the initial porosity p , the larger is the strength and stiffness, and the smaller is the material ductility. For a high value of p, the response of concrete is very brittle. Moreover, the tensile strength is more than twice bigger than in a laboratory test [9].

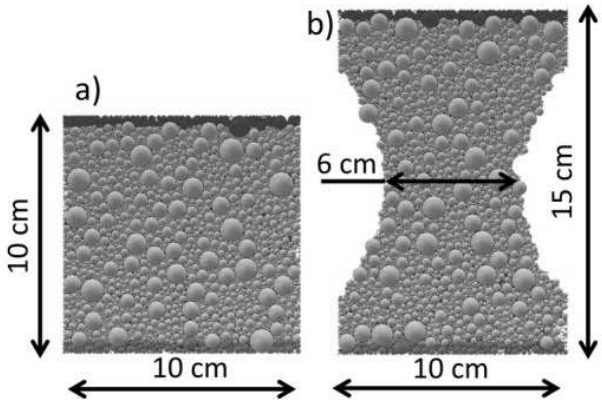

Figure 2: Specimens assumed for compression [8] (a) and tension tests [9] (b)

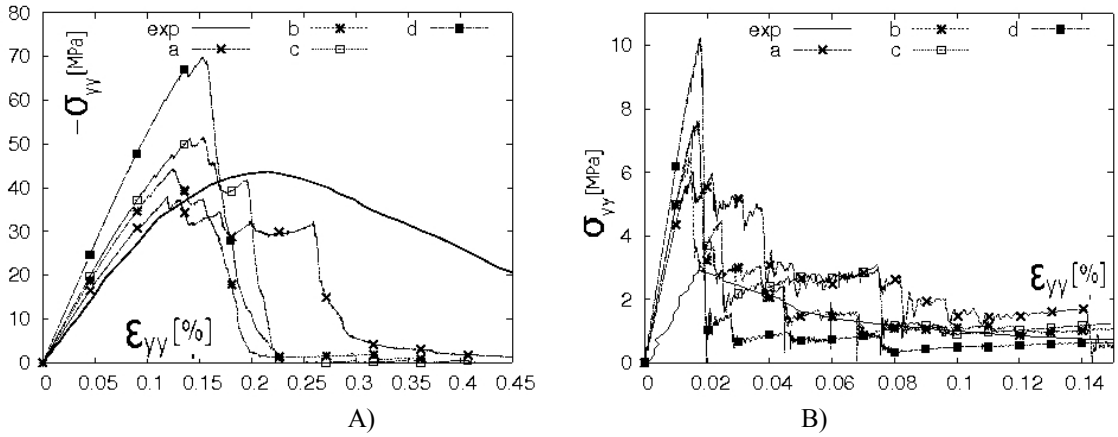

Figure 3: Calculated stress-strain curve: A) uniaxial compression or B) uniaxial tension concrete test with different initial porosity compared to experiments [8,9] ('exp), a) p=90%, b) p=95%, c) p=100% and d) p=125%

3.2 Influence of the minimum sphere size

Four different specimens were considered (d_{min}=1 mm, d_{min}=0.5 mm, d_{min}=0.25 mm and d_{min}=0.125 mm at d_{50}=2 mm and d_{max}=12mm). The number of spheres was 1356, 3992, 8791 and 23488 (with the mean number of contact for one spheres, the so-called coordination number, equal to 4.51, 4.73, 4.94 and 5.25) during compression, and 1071, 4935, 10949 and 28 862 (with the coordination number equal to 4.51, 4.74, 4.90 and 5.28) during tension. The parameters C and T were equal 160 MPa and 90 MPa, respectively.

For compression, if smaller spheres are taken (Fig.4A), the concrete response after the peak is less brittle. The stress peak and strain corresponding to the peak are almost the same. In turn, for tension, the material ductility is not affected, however the strength decreases with decreasing minimum sphere diameter d_{min} (Fig.4B). The concrete strength is too high at d_{min}=1mm (by about 50%) and at d_{min}=0.5 mm (by about 10%).

3.3 Effect of specimen depth

In order to reduce the calculation time, the specimen size was reduced: 5×5×5 cm^3 (compression) and 7.5×5×5 cm^3 (tension). The calculations were carried out with d_{max}=12 mm, d_{min}=1.0 mm, d_{min}=2 mm, C=160 MPa and T=90 MPa.

For uniaxial compression 30'074 spheres were used (the coordination number was 9.01). An increase of the contact number had a significant influence on the macroscopic response (Fig.5A). The material indicated more ductility and the stress fluctuations were smaller. The numerical material response was very similar to the laboratory test (note that during compression, the size effect is almost negligible [8]).

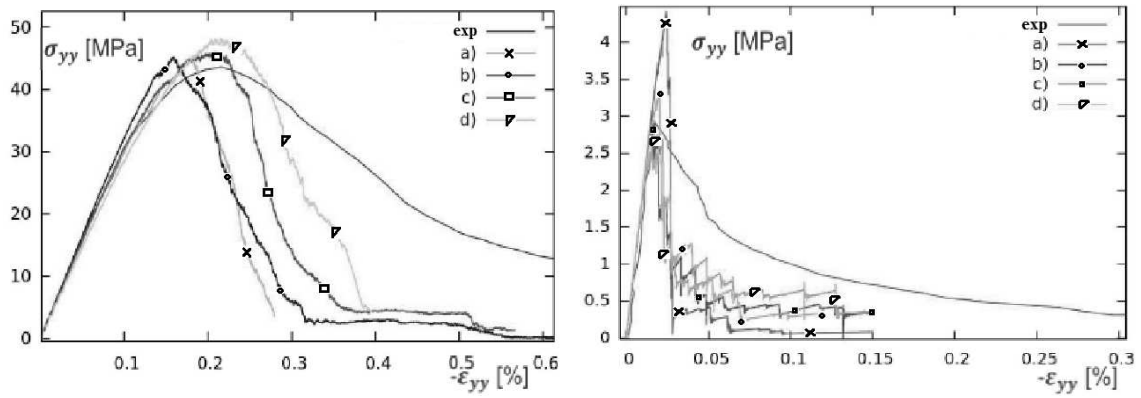

Figure 4: Calculated stress-strain curve for uniaxial compression (A) and uniaxial tension (B) with different minimum sphere diameter d_{min} compared to experiments [8,9]('exp'): a) d_{min}=1 mm, b) d_{min}=0.5 mm, c) d_{min}=0.25mm and d) d_{min}=0.125mm

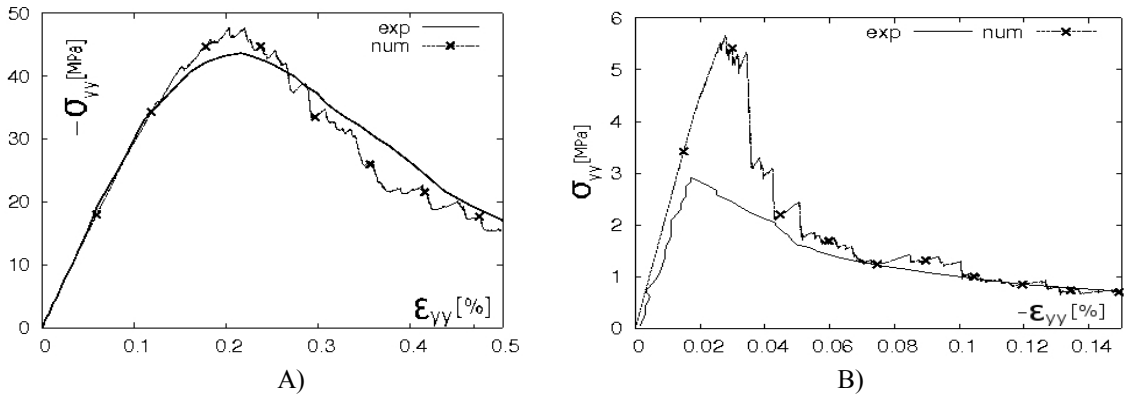

Figure 5: Calculated stress-strain curve for uniaxial compression (A) and uniaxial tension (b) concrete from 3D calculations compared to experiments [8,9] ('exp')

In the case of a 3D tensile test, 35686 spheres were used (with the coordination number equal to 9.33). The DEM results for tension (Fig.5B) show that the calculated ductility is too small due to the lack of small aggregate particles. The calculated strength is too high caused mainly by a size effect [9].

3.4 Effect of presence of ITZs

Concrete was assumed as a three-phase material by taking into account interfacial transitional zones (ITZs) between coarse aggregate and cement paste [10,11]. All spheres larger than 1mm were chosen as aggregate and spheres in the range of 5-12 mm had an interfacial zone around them (one-layer wide). All spheres below 1 mm were considered as a cement matrix. The parameters of a contact between aggregate grains with interfacial zones and cement matrix were: E_c=14 GPa, C=120 MPa and T= 60 MPa. This contact was the weakest one. Next, the contact parameters between aggregate particles without interfacial zones and cement matrix were: E_c=70 GPa, C=200 MPa and T=100 MPa (it was the strongest contact) and between spheres corresponding to the cement matrix: E_c=30 GPa, C=160 MPa and T=80 MPa. The maximum sphere diameter was d_{max}=12 mm, the smallest one d_{min}=0.25 mm and the mean diameter d_{50}=2 mm. The calculated stress-strain curves correspond well to the laboratory test results (Fig.6). The material ductility was improved. To reduce numerical stress fluctuations, the sphere number should be larger.

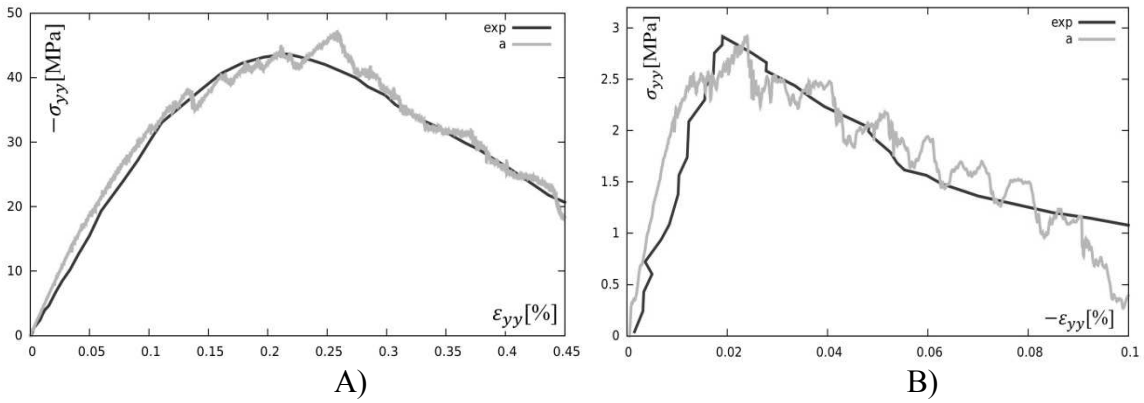

Figure 6: Calculated stress-strain curve for uniaxial compression (A) and uniaxial tension (B) for concrete described as three-phase material as compared to experiments [8,9] ('exp')

The deformed specimens from 2D DEM are shown in Fig.7. The calculated failure mechanisms are similar as in experiments. For compression, vertical and inclined cracks appear (Fig.7A), and for tension, a single crack forms in a narrower specimen region and propagates then horizontally across it (Figs.7B).

3.5 Evolution of micro-structure

The porosity distribution from 2D discrete calculations is shown in Fig.8. In turn, Fig.9 shows the maps of displacement fluctuations which were calculates as

$$\vec{\delta}_i^{mn} = (\vec{r}_i^{\,n} - \vec{r}_i^{\,m}) - \vec{u} \tag{5}$$

where $\vec{r}_i^{\,m}$, $\vec{r}_i^{\,n}$ are the positions of the sphere i in the steps m and n and $\vec{u}$ is the mean sphere displacement in the specimen. For compression, two cracks develop near the peak stress, however after the peak, the left one dominates. For tension, an almost horizontal crack starts from the left side of the specimen and propagates next to the right side.

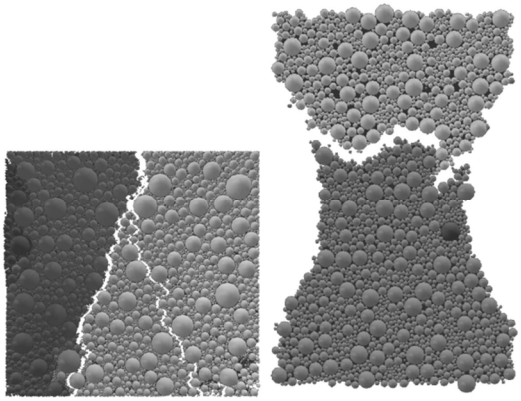

Figure 7: Deformed specimens from DEM: A) uniaxial compression and b) uniaxial tension

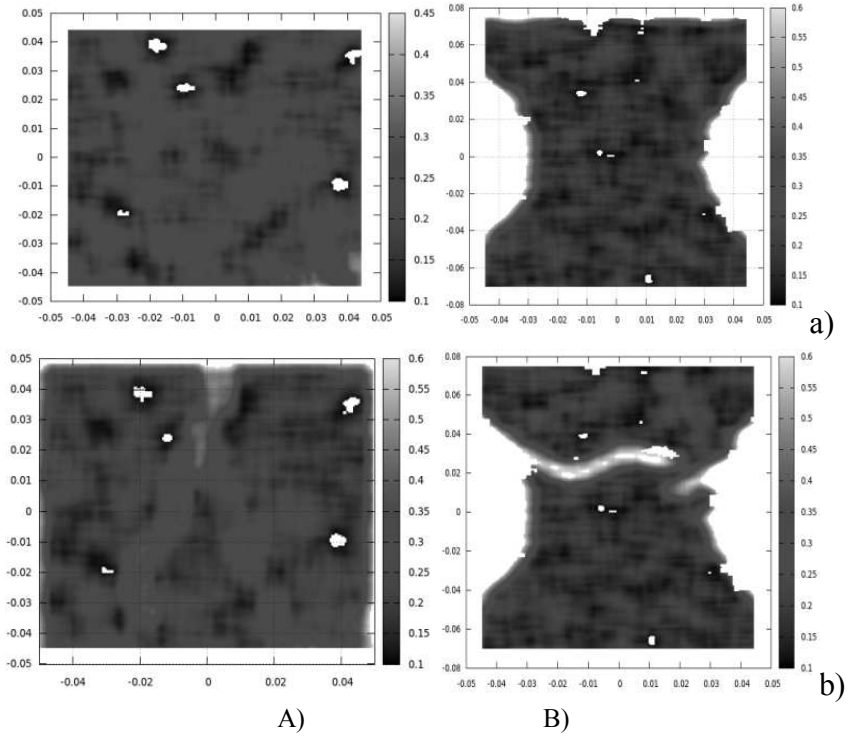

Figure 8: Calculated porosity distribution in concrete specimens during uniaxial compression (A) and uniaxial tension (B), a) before test and b) after peak stress

The evolution of a contact network in a concrete specimen is demonstrated in Fig.10. The force magnitude is expressed by the line width. The distribution of internal contact forces is non-uniform and continuously changes. Force chains of heavily loaded aggregate particles contacts bear and transmit the compressive/tensile load on the entire system and are a predominant structure of internal forces at micro-scale. They build up and collapse.

During compression, when a crack appears, vertical force chains vanish in a crack area and new vertical ones (stronger) appear on both sides of the crack (Fig.10a). For tension, force chains start to colaps on the left specimen side and stronger ones occurs on the right specimen side. When a crack is developed, force chains start to change their orientation – from a vertical one to a diagonal and a horizontal one.

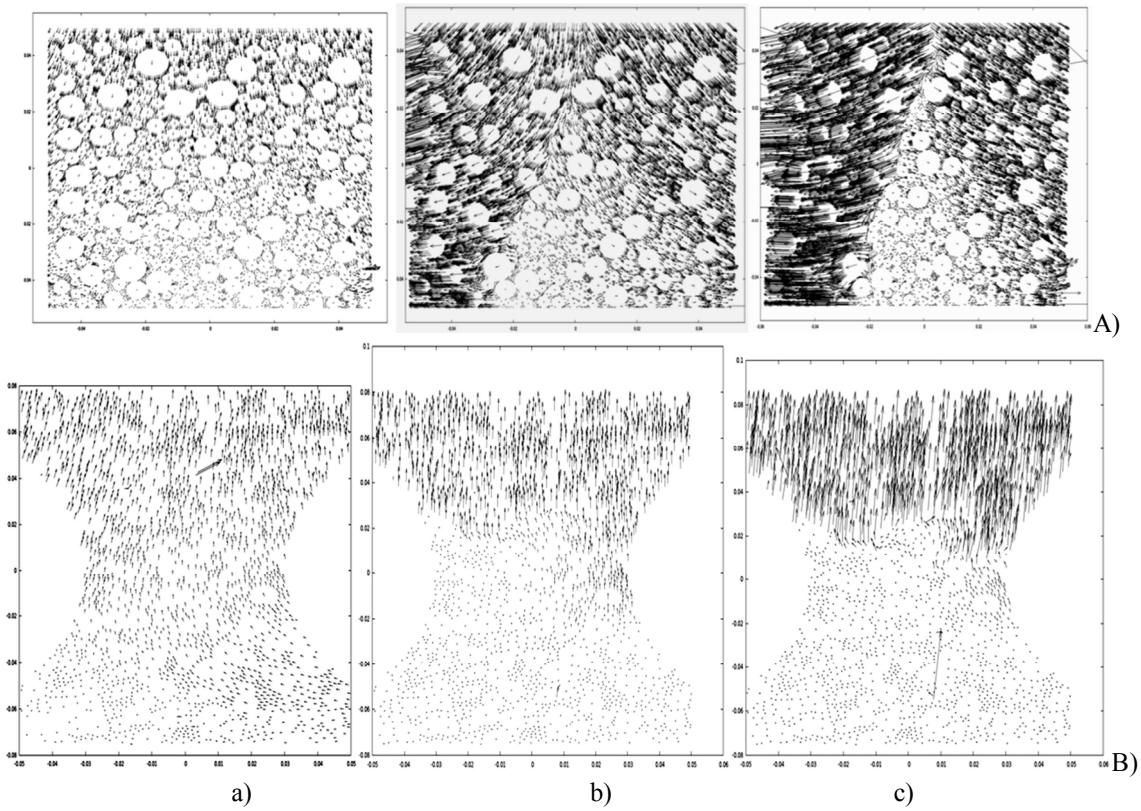

Figure 9: Calculated displacement fluctuations in concrete specimens during uniaxial compression (A) and uniaxial tension (B), a) test begin, b) close to peak stress and c) after peak stress

4 CONCLUSIONS

DEM may realistically predict experimental concrete results of uniaxial compression and uniaxial tension at the global level. The influence of 3D calculations, and presence of small aggregate particles and interfacial transitional zones are of importance. The advantage of the model is that it allows for a deep study of micro-structure changes under deformation.

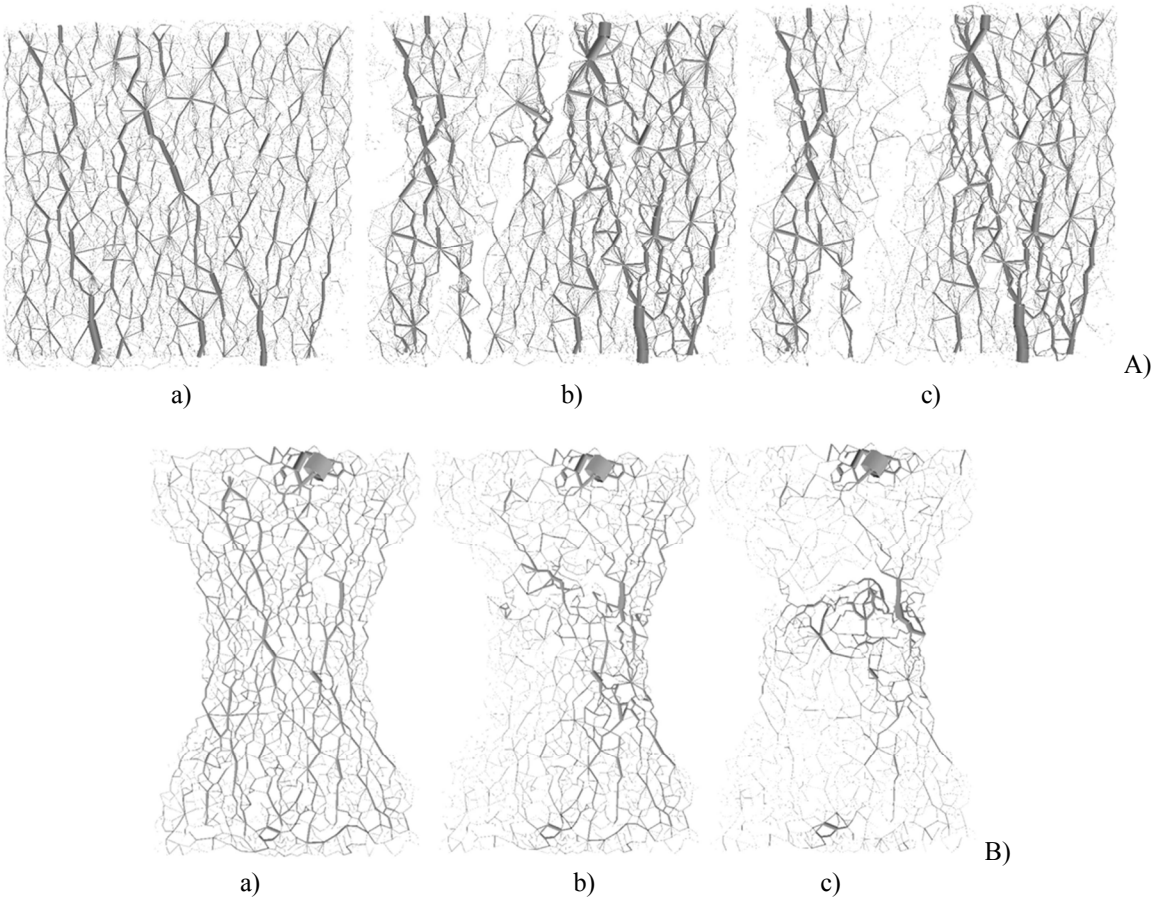

Figure 10: Distribution of contact normal forces between spheres during uniaxial compression (A) and uniaxial tension (B): a) test begin, b) close to peak stress and c) after peak stress

REFERENCES

[1] Camborde, F., Mariott, F. and Donze, F. Numerical study of the rock and concrete behaviour by discrete element modelling. *Computers and Geotechnics* (2000) **27** (4):225-247.

[2] Hentz, S., Daudeville, L. and Donze, F. Discrete element modelling of concrete and identification of the constitutive behaviour. *15th ASCE Engineering Mechanics Conference, New-York (Columbia University), Org. American Society of Civil Engineers* (2002) 777-785.

[3] Rojek, J. Discrete element modeling of rock cutting. *Computer Methods in Materials Science* (2007) 7(2):224-230.

[4] Poinard, C., Piotrowska, E., Marin, P., Malecot, Y. and Daudeville, L. Mesoscopic scale modeling of concrete under triaxial loading using X-ray tomographic images. *Proc. II International Conference on Particle-based Methods – Fundamentals and Applications* (2011).

[5] Smilaur ,V. Cohesive particle model using the Discrete Element Method on Yade platform. *PhD Thesis, Czech Technical University in Prague and Grenoble University,* (2010).
[6] Kozicki, J. and Donze, F. A new open-source software developer for numerical simulations using discrete modelling methods. *Computer Methods in Applied Mechanics and Engineering* (2008) **197**:4429-4443.
[7] Smilauer V. and Chareyer B. Yade DEM formulation. 1st edition – from release bzr2718 (2011).
[8] van Mier, J.G.M. Multiaxial strain-softening of concrete. *Materials & Structures* (1986) **19**(111):179-200.
[9] van Vliet, M.R.A. and van Mier, J.G.M. Experimental investigation of size effect in concrete and sandstone under uniaxial tension. *Engineering Fracture Mechanics* (2000) **65**:165-188.
[10] Lilliu, G. and van Mier, J.G M. 3D lattice type fracture model for concrete. *Engineering Fracture Mechanics*, (2003) **70**:927–941.
[11] Kozicki, J. and Tejchman, J. Effect of aggregate structure on fracture process in concrete using 2D lattice model. *Arch. Mech*. (2007) **59**(4–5):365–384.